Carbon Monoxide and Soot Emissions from Liquid-Fueled Buoyant Turbulent Diffusion Flames

Ü. Ö. KÖYLÜ and G. M. FAETH*

Department of Aerospace Engineering, The University of Michigan, Ann Arbor, MI 48109-2140 USA

Carbon monoxide concentrations, soot concentrations, and mixture fractions were measured in the fuel-lean (overfire) region of liquid-fueled buoyant turbulent diffusion flames burning in still air. Pool-fire configurations were studied with the liquids burning from horizontal round wicks, considering both sooting (toluene, benzene, *n*-heptane, and isopropanol) and nonsooting (methanol and ethanol) fuels. Flame heights and characteristic residence times also were measured, both for the turbulent flames and at the normal smoke point (for the sooting fuels). Carbon monoxide and soot generation factors (mass of CO or soot emitted per unit mass of fuel carbon burned) were uniform throughout the overfire region and were relatively independent of flame residence times (which were generally an order of magnitude longer than the normal smoke point residence times of the sooting fuels). Processes of carbon monoxide and soot emission for the nonalcohols are closely related, based on the good correlation between their emission factors: 0.37 kg CO/per kg soot with a standard deviation of 0.09. However, nonsooting methanol and ethanol/air flames still emitted low levels of CO so that there is a component of CO emissions that is not associated with soot.

NOMENCLATURE

g	acceleration of gravity
C_p	specific heat at constant pressure
d	burner exit diameter
d_p	soot particle effective optical diameter
f	mixture fraction
f_s	soot volume fraction
L	flame height
L_s	flame height at laminar smoke point
$\dot{m}_f$	fuel mass flow rate
$\dot{m}_{fs}$	fuel mass flow rate at laminar smoke point
M_i	molecular weight of substance i
$\dot{Q}_f$	flame heat release rate
Q^*	dimensionless heat release parameter (Eq. 1)
r	radial distance
Ri	burner Richardson number, gd/u_0^2
t_r	characteristic flame residence time
t_s	characteristic residence times at laminar smoke point
t^*	dimensionless residence time parameter (Eq. 2)
T	temperature
u	streamwise velocity
x	height above burner
X_i	mole fraction of species i
Y_i	mass fraction of species i

Greek Symbols

η_{CO}	carbon monoxide generation factor
$\eta_{CO/s}$	carbon monoxide/soot generation correlation
η_s	soot generation factor
λ	wavelength of light
ρ	density
ρ_s	density of soot

Subscripts

c	flame axis
q	conditions where soot oxidation quenches
o	burner exit condition
∞	ambient condition

INTRODUCTION

The present investigation considers the emissions of carbon monoxide and soot, as well as the correlation between these emissions, for liquid-fueled buoyant turbulent diffusion flames typical of overventilated natural fires. The correlation between these emissions is important because they

* Corresponding author

0010-2180/91/$3.50

both are major contributors to hazards: inhalation of carbon monoxide is the main cause of fire fatalities, continuum radiation from soot increases fire growth and burning rates, and soot-laden smoke obscures fire fighting efforts. Many workers have noted a correlation between carbon monoxide and soot emissions, suggesting a synergism of these hazards that has important implications concerning materials properties for improved fire safety [1–6]. Earlier work in this laboratory confirmed this behavior for buoyant turbulent diffusion flames involving gaseous alkane, alkyne, and alkene fuels burning in still air [7, 8]. The present study extends this work to a broader range of hydrocarbons, including aromatics and alcohols, by considering liquid fuels in pool-like flame configurations.

The discussion of past work is brief because carbon monoxide and soot emissions from buoyant turbulent diffusion flames recently were reviewed by Köylü et al. [8]. Buoyant turbulent diffusion flames generally have modest stretch rates so that concentrations of major gas species satisfy the laminar flamelet concept [9], where concentrations of major gas species are correlated solely as a function of mixture fraction (or fuel-equivalent ratio) called state relationships. Measurements in laminar flames have provided state relationships for a number of fuels burning in air, including soot-containing flames, which have been applied with some success to estimate scalar properties in turbulent flames; see Ref. 10 and citations therein. Although these generalized correlations show large concentrations of CO for fuel-rich conditions, they generally exhibit low concentrations of CO for fuel-lean conditions which contradicts observations of CO emissions from turbulent flames [1–5, 8]. This behavior has been explained by the limited sensitivity of CO measurements used to find state relationships and the possibility that CO being emitted from flames largely accompanies soot within the soot layer as it passes from fuel-rich to fuel-lean conditions—a region that generally is not considered when state relationships are measured due to problems of soot clogging sampling systems [8]. Recent measurements within laminar flames tend to support the latter explanation, showing levels of CO higher than estimates from state relationships within fuel-lean portions of the soot layer [6].

Earlier work in this laboratory examined both CO and soot emissions from gas-fueled (acetylene, propylene, ethylene, propane, and methane) buoyant turbulent diffusion flames burning in still air [7, 8]. Emissions were represented by generation factors, η_{CO} and η_s, defined as the mass of CO or soot emitted per unit mass of fuel carbon burned. (This differs from CO or soot yields defined in Refs. 2 and 3, which are the mass of CO or soot emitted per unit mass of fuel burned.) It was found that CO and soot generation factors were relatively independent of position in the overfire region, that they tended to increase with increasing flame residence time, that they eventually reached relatively constant asymptotic values at residence times roughly an order of magnitude longer that the laminar smoke point residence time, and that emissions of CO and soot were strongly correlated (except for methane, which was nonsooting), yielding $\eta_{CO} = 0.34\ \eta_s$. This established a strong correlation between mechanisms producing CO and soot in these flames, supplemented by a weaker mechanism not involving soot to explain measurable but low levels of CO emissions from nonsooting methane flames.

The objective of the present investigation was to determine whether the trends concerning CO and soot emissions from gas-fueled buoyant turbulent diffusion flames [7, 8] extended to a broader class of hydrocarbons accessible as liquid fuels. Fuels considered included aromatics (toluene and benzene), a heavy saturated hydrocarbon (*n*-heptane) and three alcohols (isopropanol, ethanol, and methanol). Ethanol and methanol were of interest to highlight the nonsooting CO emission mechanism because flames with these fuels did not emit soot for present test conditions. Measurements included the following properties for the turbulent flames: soot and CO concentrations in the overfire region, soot and CO emission factors and their correlation, flame lengths, and flame residence times. Measurements also were made of laminar smoke point flame lengths and residence times. The measurements of CO and soot properties were needed for the direct objectives of the study, while measurements of flame lengths and residence times help characterize present test conditions and their relationship to the long residence time regime.

EXPERIMENTAL METHODS

Turbulent Flame Apparatus

The overall test arrangement was similar to the earlier gas-fueled experiments [7, 8], aside from different burner systems to accommodate liquid fuels. The present experiments involved burning from round, horizontal, fuel-soaked wicks that were facing upward. Combustion was in still air with the wicks located near the axis of a large enclosure (2.4 × 2.4 × 3.6 m high). The enclosure had a metal hood at the top and an adjustable exhaust system to collect and remove combustion products without disturbing the flames. Room disturbances of the flames were minimized by using strips of plastic film, terminating near the floor, as the side walls of the enclosure, and a second smaller screened enclosure (1 × 1 × 2 m high, open at the top) directly around the flames. Instrumentation was mounted rigidly so that the burner was traversed horizontally and vertically (with positioning accuracies of 0.1 and 1 mm, respectively) to make measurements at various points within the fuel-lean (overfire) region of the flames.

Figure 1 is a sketch of the burner assembly. Fuel was supplied to the flames from round fuel-saturated wicks (Carborundum Co., Duraboard KBLD162436, 25 mm thick). The wicks were mounted level with the top of close-fitting stainless-steel pans so that burning from the sides of the wicks was inhibited. Three burner (wick) diameters were considered: 50, 125, and 195 mm. This allowed evaluation of effects of scale while maintaining turbulent flames of reasonable size so that properties could be measured in the cool portions of the plume.

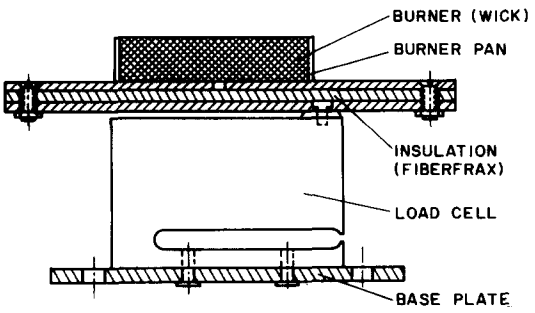

Fig. 1. Sketch of the burner assembly.

Heat soak-back to the wick assembly caused gradual increases of the burning rate with time. Therefore, burning rates were monitored so that they could be known in the period when measurements were made. This was done by mounting the wick burner pans on a load cell (Interface, Model SPI-15, single-point type, 6.8 kg capacity). Thermal disturbances of the load cell were controlled by an insulated barrier at the bottom of the burner pan. The output of the load cell was amplified and then stored and processed with a microcomputer. The arrangement was calibrated using weights of known mass. Experimental uncertainties (95% confidence) of the burning rate measurements for the turbulent flames were less than 5%.

Laminar Smoke Point Apparatus

Laminar smoke point properties of the liquid-fueled flames were measured to establish long residence time conditions for the present flames. This involved use of the same wick system as the turbulent flame tests but with much smaller wick diameters: 5–25 mm in increments of 5 mm with wick thicknesses of 25 mm. These tests also involved burning in still air within a screened enclosure to control room disturbances.

The small-diameter wicks exhibited progressively decreasing burning rates and flame heights with time. Thus, the procedure to find laminar smoke points involved selecting a wick diameter where the flame emitted soot at first but eventually reached the smoke point as the flame became shorter. The laminar smoke point was defined in the same manner as Schug et al. [11], as the point where the tips of the small luminous protuberance from the soot layer (the "wings") coincided with the tip of the flame.

The flame height at the laminar smoke point was measured from flame photographs, as is described later. Flame height determinations largely were limited by exactly specifying protuberance and flame heights and disturbances of the longer flames. In view of these factors, experimental uncertainties (95% confidence) of laminar smoke point flame heights are estimated to be less than 10%.

The effect of burner diameter on the laminar smoke point flame height also was examined. For

the range of diameters that could be considered for a particular fuel using present methods (generally less than 2:1), the burner diameter did not affect the smoke point flame height within experimental uncertainties.

Instrumentation

Flame Photography

In addition to monitoring the burning rate, the turbulent flames were characterized by measuring their flame heights and characteristic residence times similar to Ref. 7. Except for methanol, the test flames were luminous and were readily photographed in a darkened room for these determinations. This involved motion picture photographs (200–1000 pps using 16-mm Kodak 4X film) with 100- and 1000-Hz timing marks on the film, depending on conditions.

Flame height measurements were obtained by averaging luminous flame heights (taken as the highest position where luminosity was observed) on 100 pictures, obtained over a 5–10-s period. The experimental uncertainties (95% confidence) of the flame heights are estimated to be less than 10%.

Characteristic flame residence times (called "residence times" in the following) were defined in the same manner as in Ref. 7, as the time interval between interruption of the fuel flow and the disappearance of all flame luminosity. These measurements were made for both the turbulent flames and at the laminar smoke points. The fuel flow rate was terminated by a pneumatically driven shutter passing across the burner a few millimeters above its surface. Shutter speeds allowed the leading edge of the shutter to cross the burner exit in less than 2–40 ms for the 5–195-mm-diameter burners. Camera speeds yielded less than 2 and 10 ms discretization errors on the films for the laminar and turbulent flames. Ten tests were averaged to find the characteristic residence time for each flame condition to yield experimental uncertainties (95% confidence) estimated to be less than 20% for the laminar flames and 10% for the turbulent flames.

Optical/Sampling Probe

Mean soot volume fractions and mixture fractions were measured simultaneously using the optical/sampling probe described in Ref. 7. These measurements were limited to the far overfire region (mean fuel-equivalence ratios less than 4×10^{-3} and mean temperatures less than 450 K), where relationships between mean and instantaneous scalar properties are the same. The system involves drawing a sample into a 25 × 25 mm passage where mean soot volume fractions are measured by laser extinction, and mean mixture fractions are measured by gas chromatography. Sampling was not isokinetic (velocities were unknown); however, effects of doubling and halving sampling rates were negligible.

The 632.8-nm line of a HeNe laser was used for the extinction measurements, with the beam making 16–18 passes across the sample to achieve extinction levels needed for acceptable experimental uncertainties. The extinction ratio was obtained by averaging ten groups of 5000 samples, each obtained over a 10-s period.

Past multiline laser extinction measurements within the fuel-rich (underfire) region of acetylene and ethylene flames suggest that effective optical size parameters of soot particles, $\pi d_p/\lambda$, are less than 0.5 at a wavelength of 632.8 nm [12, 13], so that discrepancies between Rayleigh and Mie scattering predictions of soot volume fractions are less that 15% [14]. Thus, to provide a common basis of comparison with earlier work [2, 3, 6, 7], soot volume fractions were inferred from the laser extinction measurements assuming Rayleigh scattering and using the soot refractive index measurements of Dalzell and Sarofim [15], i.e., $1.547-0.56i$ at 632.8 nm. Due to the simplicity of the Rayleigh scattering relationship between soot volume fraction and laser extinction [14], this approach also has the advantage that present results can be readily corrected if new information about the scattering properties of overfire soot for the present fuels becomes available.

Aside from uncertainties about the Rayleigh scattering approximation and the appropriate refractive indices of soot, experimental uncertainties of soot volume fractions were largely controlled by the magnitude of the laser extinction ratio and finite sampling times: they are estimated (95% confidence) to be less than 30% for soot volume fractions greater than 2×10^{-3} ppm, which was the lowest value considered during the tests.

Samples for gas composition and mixture fraction measurements were filtered to remove water vapor so that analysis was on a dry basis. The arrangement and operating conditions of the gas chromatograph, and methods of data reduction, were the same as Gore [16]. Experimental uncertainties (95% confidence) are estimated to be less than 10% for the concentrations of major gas species and less than 20% for mixture fractions.

Gas Sampling Probe

Carbon monoxide concentrations and mixture fractions were measured simultaneously using the same arrangement as Ref. 8. The approach is described completely herein because few details are provided in Ref. 8. The CO measurements were made in the far overfire region at the same locations as the soot volume fraction measurements. Sampling involved an uncooled 5-mm-diameter probe because the low temperatures (less than 450 K) assured a passive environment. No attempt was made to sample isokinetically because only relationships between CO concentrations and mixture fractions were sought.

An NDIR analyzer (Beckman, Model 867) was used for the CO measurements. The sample was dried and filtered before entering the analyzer to reduce uncertainties from the presence of water vapor and particulates. The sampling train included the following components: a coil condenser constructed of 5-mm-diameter tubing, 1500 mm long, within an ice bath; a trap and in-line filter to remove condensate and particles having sizes greater than 5 μm; a HEPA capsule filter (Gelman 12144) having a diameter of 59 mm and a length of 185 mm to remove particles larger than 0.3 μm with 99.96% efficiency; a drying unit (Nalgene 6201-0080) 200 mm long containing 20 g calcium chloride; a Drierite indicating drying tube (Grainger 17838) to serve as a second drying column; a diaphragm pump; a rotameter to monitor sample flow rates; and finally the NDIR analyzer. Flow rates through the sampling train were in the range 50–60 ml/s to provide proper instrument operation and reasonable purging times.

Present CO concentrations were in the range 1–200 ppm and were found using the lowest three ranges of the NDIR analyzer (0–50, 0–200 and 0–1000 ppm). The analyzer was calibrated before and after testing each day using prepared gas mixtures (Scott Specialty Gases: 10.10, 99.93, 949.3, 2299 ppm of CO in air; 4.97 and 13.91% CO_2 in air). The output of the analyzer was stored and processed using a microcomputer, sampling at 250 Hz and averaged over 40s, repeating and averaging over ten such intervals to achieve day-to-day repeatability within 10%. The sampling system was purged with CO-free air between each measurement until baseline zero values were retrieved.

Experimental uncertainties of the CO measurements were dominated by limited sensitivity due to the overlap of the infrared gas bands of CO and CO_2 and finite sampling times: they are estimated (95% confidence) to be less than 10% for concentrations greater than 10 ppm, increasing inversely with concentration for lower values. Methods of measuring mixture fractions, and the uncertainties of these measurements, were the same as for the optical/sampling probe.

Test Conditions

Test conditions are summarized in Table 1. Richardson numbers are based on burner exit conditions finding the velocity from the measured burning rate while assuming that the density of the mixture was equal to the fuel density at the normal boiling point. The Richardson numbers are generally in excess of 5000, which is representative of strongly buoyant flames. All the flames were turbulent, except near their base. Ranges of other properties of the flames were comparable to the gas-fueled buoyant turbulent flames of Refs. 7 and 8: heat release rates of 2.3–20.5 kW, flame lengths of 190–650 mm, and residence times of 126–532 ms. Flame heights and residence times could not be measured for methanol by present methods because light emission from these flames was too weak; therefore, the values in Table 1 for methanol were estimated using correlations that are discussed later. Measurements were made at various heights above the burner, x/d of 3.6–35.0, both at the axis and at r/x of 0.06 and 0.012 so that flows leaving various points along the flame sheet could be studied.

Present measurements of laminar smoke point properties of the fuels are summarized in Table 2. The burning rates for these tests were too small to be measured using present methods; therefore,

TABLE 1

Summary of Test Conditions[a]

d (mm)	Ri[b]	$\dot{m}_f$ (mg/s)	$\dot{Q}_f$ (kW)	L (mm)	t_t^c (ms)	x/d[d]
Toluene (ρ_0 = 3.11 kg/m^3)						
50	6270	54	2.3	295	279	14.2-35.0
125	15450	340	14.4	520	531	7.6-16.7
Benzene (ρ_0 = 2.69 kg/m^3)						
50	3150	66	2.7	280	273	14.2-35.0
125	10930	350	14.1	525	510	7.6-16.7
n-Heptane (ρ_0 = 3.29 kg/m^3)						
50	11040	43	1.9	275	212	10.8-19.0
125	58230	185	8.2	450	412	6.5-11.5
195	87010	460	20.5	650	532	7.4-9.4
Isopropanol (ρ_0 = 2.06 kg/m^3)						
50	5860	37	1.2	190	126	10.8-14.2
125	30610	160	5.3	370	324	5.6-6.5
195	47600	390	12.9	510	495	7.4-8.3
Ethanol (ρ_0 = 1.60 kg/m^3)						
125	19350	156	4.2	290	245	5.6-7.6
195	36140	347	9.3	395	412	3.6-4.9
Methanol (ρ_0 = 1.15 kg/m^3)						
125	10320	155	3.1	260[e]	224[f]	4.5-6.5
195	19130	345	6.8	330[e]	335[f]	3.6-4.9

[a] Combustion from a round horizontal wick in still air at normal temperature and pressure.
[b] Ri = gd/u_0^2 using the fuel vapor density at normal boiling point to estimate u_0.
[c] Time between termination of fuel flow and disappearance of all flame luminosity.
[d] Measurements at r/x = 0.00, 0.06 and 0.12 for this range of x/d.
[e] Calculated from correlation of Zukoski et al. [17], Eq. 2.
[f] Calculated from present residence time correlation, Eq. 5.

only qualitative values are given in the table for reference purposes, computed following Zukoski et al. [17] from the present flame length measurements. Laminar smoke point flame heights and residence times, however, were measured as described earlier. Laminar smoke point flame lengths for burning in an air coflow, from Olson et al. [18], found using a cylindrical fuel-saturated wick, and Clarke et al. [19], found by increasing the liquid pool diameter in a funnel-shaped fuel reservoir, also are summarized in Table 2. Due to the different test methods, values of L_s from the three studies only agree qualitatively, e.g., variations of preheating for different wick designs and various levels of coflow cause variations of L_s [11].

TABLE 2

Laminar Smoke Point Properties[a]

Fuel	Toluene	Benzene	*n*-Heptane	Isopropanol
Present Study:				
d (mm)	5	5	20	25
$\dot{m}_{fs}$ (mg/s)[b]	0.05	0.06	4.6	8.0
$\dot{Q}_f$ (W)[b]	2.1	2.4	205	264
L_s (mm)	17	18	106	118
t_s (ms)	13	15	41	49
Olson et al. [18]:				
$\dot{m}_{fs}$ (mg/s)	0.27	—	5.13	—
L_s (mm)	7	—	125	—
Clark et al. [19]				
L_s (mm)	10	9	159	179

[a] Combustion of liquid fuel in air at normal temperature and pressure.
[b] Calculated from correlation of Zukowski et al. [17], Eq. 2.

In spite of quantitative differences among the three determinations of L_s listed in Table 2, there is general agreement about the order of the propensity to soot: toluene and benzene about the same with *n*-heptane and isopropanol having progressively weaker tendencies to soot. In addition, methanol and ethanol did not emit soot for any laminar flame condition using present test methods. Furthermore, none of the turbulent methanol and ethanol flames emitted any soot, based on extensive measurements with the optical/sampling probe as well as thermophoretic sampling

for long time periods and observations using TEM.

Laminar smoke point residence times in Table 2 increase in the same order as L_s. For the sooting fuels, the turbulent flames have t_r/t_s in the range 2.6–41, which corresponds to the long residence time regime where emissions of soot and CO were relatively independent of flame residence time for the gaseous fuels [7, 8].

RESULTS AND DISCUSSION

Flame Heights

Flame heights and residence times will be considered first in order to help characterize the test conditions. Flame heights for the three burners and all the fuels except methanol (where the flame heights could not be observed, as noted earlier) are illustrated in Fig. 2. The results are plotted according to the scaling relationships of Zukoski et al. [17] for buoyant flames. This involves plotting L/d as a function of the dimensionless heat release parameter.

$$Q^* = \dot{Q}_f/(\rho_\infty C_{p\infty} T_\infty g^{1/2} d^{5/2}). \quad (1)$$

Measurements for the gas-fueled buoyant turbulent diffusion flames, studied earlier [7], along with several other sets of measurements for a variety of gas, liquid, and solid fuels [17, 20–22], are also shown on the plot.

The present flame height measurements in Fig. 2 are in excellent agreement with those of Sivathanu and Faeth [7] and Zukoski et al. [17], which involved different burners but similar measuring techniques. The flame length determinations of Refs. 20–22 are somewhat longer probably because they are based on direct visual observations. However, the differences among all the measurements are not large in view of the subjective nature of the fluctuating visible length

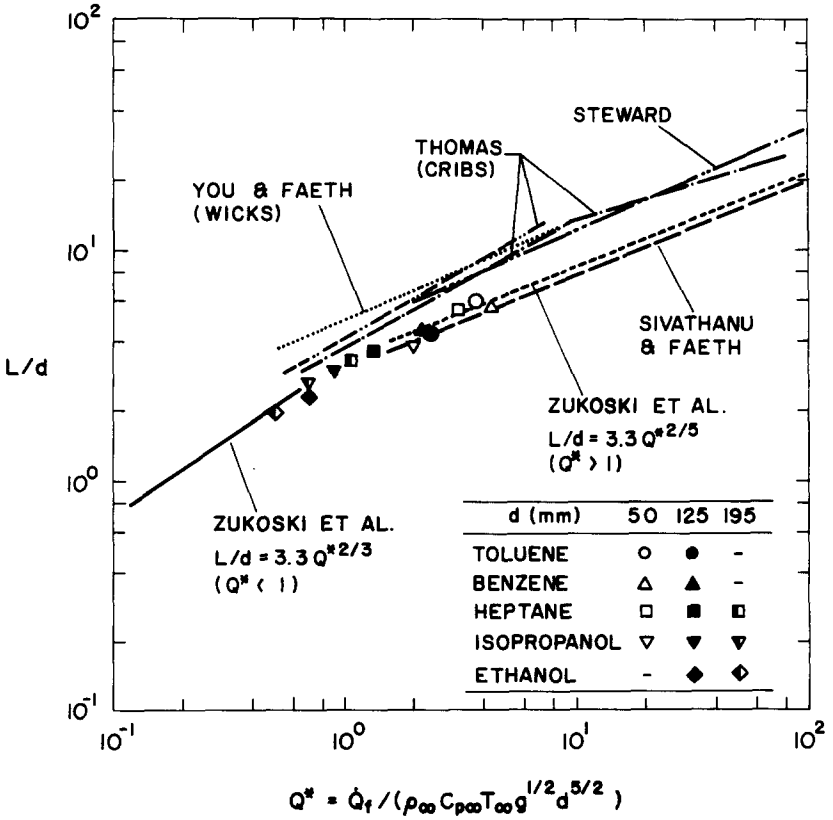

Fig. 2. Flame heights as a function of heat release rate for buoyant turbulent diffusion flames. Other data from Sivathanu and Faeth [7], Zukoski et al. [17], Steward [22], Thomas [21], and You and Faeth [22].

of a turbulent diffusion flame. Thus, the present flames are typical of buoyant pool fires and their lengths are reasonably correlated by the expression proposed by Zukoski et al. [17]:

$$L/d = 3.3Q^{*2/3}, \quad Q^* < 1;$$
$$L/d = 3.3Q^{*2/5}, \quad Q^* \geq 1. \tag{2}$$

Due to the reasonable agreement between present measurements and Eq. 2, it was used to estimate L for the turbulent methanol flames in Table 1, and $\dot{Q}_{fs}$ and $\dot{m}_{fs}$ from the measured value L_s at the laminar smoke points in Table 2.

Residence Times

Flame residence times are important in order to estimate approach to the long residence time regime. A correlation of this property was developed in Ref. 7; however, this approach was not effective for present measurements and it was revised. The present procedure was to associate the characteristic flame residence time with the time required for a fluid parcel to pass from the burner exit to the mean tip of the flame, as follows:

$$t_r \sim \int_0^L u_c^{-1}\, dx. \tag{3}$$

Drysdale [23] indicates that velocities along the axis of buoyant turbulent flames can be correlated as follows:

$$u_c \sim \left(g\dot{Q}_f/\rho_\infty C_{p\infty} T_\infty x\right)^{1/3}. \tag{4}$$

Substituting Eq. 4 into Eq. 3 and completing the integration yields an expression for the residence time in terms of the flame length. Eliminating the flame length from this expression, using the correlations of Eq. 2, and selecting the constant of proportionality resulting from Eqs. 3 and 4 to best match the present data and that of Ref. 7, yields the following residence time correlations:

$$t^* = 2.9Q^{*5/9}, \quad Q^* < 1;$$
$$t^* = 2.9Q^{*1/5}, \quad Q^* \geq 1, \tag{5}$$

where

$$t^* = t_r(g/d)^{1/2}. \tag{6}$$

Values of t^* are plotted as a function of Q^* in Fig. 3. Measurements are shown for the present liquid-fueled flames and for the buoyant gas-fueled flames of Ref. 7, along with the correlations of Eq. 5. The correlations yield the trends of the data reasonably well and quantitative agreement is within experimental uncertainties except for the results for acetylene. The values of t^* for acetylene generally are 20% lower than the rest but the reasons for this behavior are not known; notably, the approach of Ref. 7 provides a better correlation of the acetylene results. Nevertheless, the correlations of Eq. 5 provide a convenient estimate of residence times that is consistent with the flame length correlations of Zukoski et al. [17] (Eq. 2). These expressions were used to estimate t_r for the methanol flames in Table 1 because weak flame luminosity prevented direct measurement of t_r by present methods, as noted earlier.

Equation 5 provides some insight about the scaling of present residence times to practical fires. For larger flames, $Q^* > 1$ and the residence time is proportional to $\dot{Q}_f^{1/5}$ and is independent of d. Thus, residence times only increase by roughly a factor of 2 when burning rates are increased from the larger flames of Table 1 to the MW range of practical fires.

Soot Properties

The present optical/sampling probe measurements were limited to the far overfire region where differences between time-averages and mass-weighted (Favre) averages are small, and where relationships between time-averaged and instantaneous scalar properties are identical. Furthermore, soot oxidation in the fuel-lean region quenches near the luminous flame [24] so that soot behaves like a passive scalar in the overfire region. Then variations of soot volume fractions only are caused by variations of soot concentrations at the point where soot oxidation reactions quench and the extent of mixing with the surrounding air.

Under these circumstances, adopting the usual approximations of the conserved-scalar formalism, and assuming that properties when soot reactions quench are independent of position in the flame, yields a simple expression (or state relationship) for soot concentrations in the overfire

region. In particular, effects of preferential diffusion, kinetic energy, and radiative heat loss are ignored; soot concentrations are represented by their volume fractions; and the volume occupied by soot is neglected when computing mixture density. These are reasonable assumptions for the overfire region of the present flames. Reynolds numbers are relatively high so that turbulent mixing dominates and the low molecular diffusivity of soot has little effect. Additionally, temperatures are moderate and velocities are relatively high over most of the overfire region so that radiation numbers are small. Finally, soot volume fractions are generally less than 1 ppm so that the volume of soot can be neglected when finding the mixture density with little error. Then, the state relationship for soot volume fraction is as follows:

$$f_s = \rho f (f_s/\rho f)_q, \tag{7}$$

where the subscript q denotes conditions where soot oxidation quenches. Under the approximations of the conserved scalar formalism, ρ only is a function of f so that f_s only is a function of f for given quenching conditions as well.

Motivated by Eq. 7, the present measurements of soot volume fractions are plotted as a function of mixture fraction in Fig. 4. Results are only shown for the sooting fuels: toluene, benzene, *n*-heptane, and isopropanol. As noted earlier, no soot was detected in the overfire region of the present methanol and ethanol flames. To avoid cluttering the figure, symbols only are identified by the fuel and the burner size: the measurements also involved a range of positions in the overfire region as noted in Table 1. Finally, toluene and benzene emitted large quantities of soot and had high flame radiation levels due to continuum radiation from soot; therefore, it was difficult to make measurements with these flames for the largest burner and only the two smaller burners were used. All three burners, however, were used for the more lightly sooting *n*-heptane and isopropanol flames.

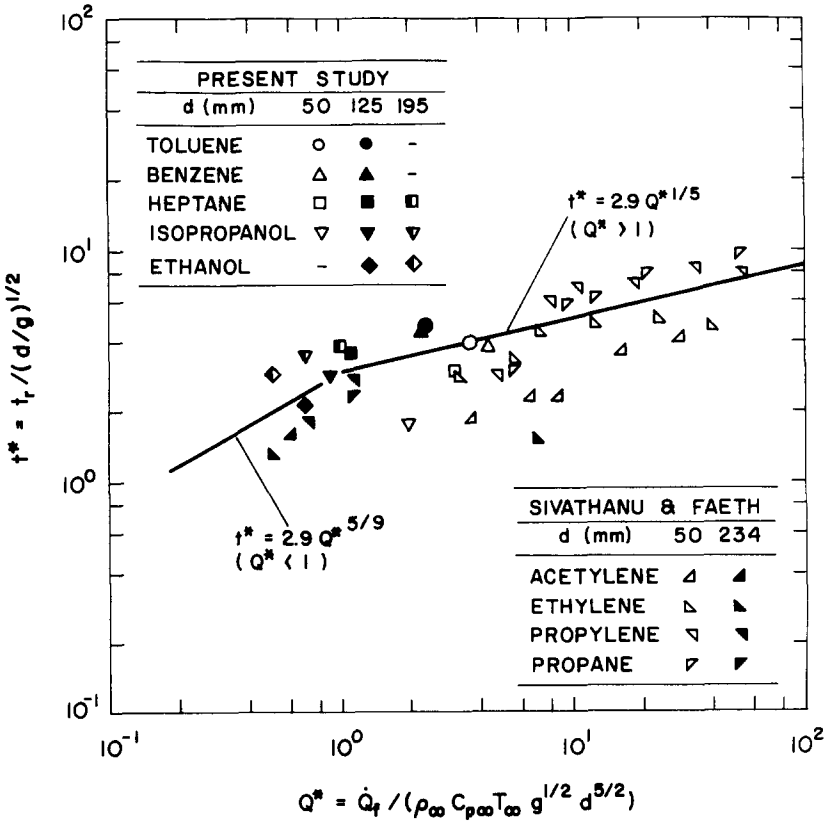

Fig. 3. Characteristic flame residence times as a function of heat release rate for buoyant turbulent diffusion flames. Other data from Sivathanu and Faeth [7].

The soot volume fraction measurements illustrated in Fig. 4 for each fuel generally fall along correlations of the best fits of the data constructed according to Eq. 7. The correlations are nearly straight lines in Fig. 4 because present test conditions involve relatively low mixture fractions, less than 4×10^{-3}, where variations of density with f in Eq. 7 are small. Noting that results for a particular symbol involve various positions in the overfire region for particular flames, it is evident that these results correlate quite well assuming passive mixing and constant conditions when soot oxidation quenches at various points within the flame. Except for isopropanol, there is a tendency for soot volume fractions to increase slightly with increasing burner size (this is most evident for toluene and benzene). Although this trend is consistent, the effect is not large in comparison to present experimental uncertainties. The results illustrated in Fig. 4 also correlate quite well with sooting tendencies based on laminar smoke point flame lengths: at a given value of f, f_s for toluene and benzene are comparable with progressively decreasing f_s for n-heptane and isopropanol.

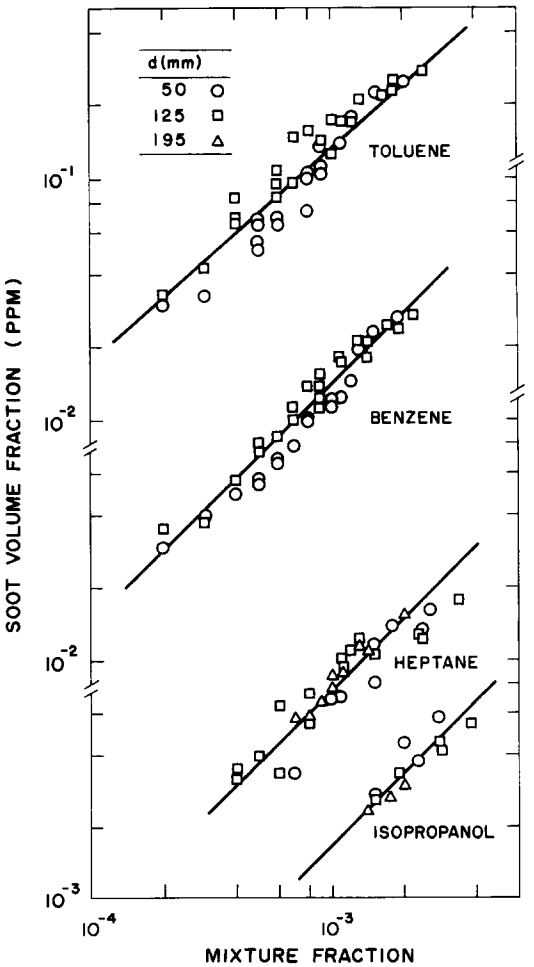

Fig. 4. Soot volume fraction state relationships for the overfire region of turbulent toluene, benzene, n-heptane, and isopropanol diffusion flames burning in air. Note that n-heptane and isopropanol are on the same cut of the plot.

The results illustrated in Fig. 4 suggest that soot properties when soot oxidation quenches are relatively independent of position within a given flame, and that subsequent variations of f_s are due to passive turbulent mixing within the overfire region of a given flame as represented by Eq. 7. Then, the emission of soot from a given flame can be represented conveniently by the soot generation factor, η_s. Analogous to the evaluation of f, η_s was found by assuming that H/C ratios were the same as the original fuel in the regions where measurements were made. Then noting that CO and soot concentrations are small in comparison to CO_2 concentrations in the far-overfire region, η_s can be found from the measured values of f_s and Y_{CO_2} as follows:

$$\eta_s = M_{CO_2}\rho_s f_s / \left(M_C \rho Y_{CO_2}\right). \tag{8}$$

For consistency with past work [7, 8], a constant soot density of 1100 kg/m^3 from Newman and Steciak [25] was used for these computations: given an alternative value of ρ_s, corrections of present results are easily made as a simple ratio. The mixture density in Eq. 8 depends on the mixture fraction, which is known for each test condition, and the degree of heat loss from the present flames. Radiative heat loss fractions of the gas-fueled buoyant turbulent diffusion flames varied with the fuel but not the flame operating condition [7], typical of buoyant flames [26]; therefore, the present flames were assumed to behave in the same manner. Additionally, the radiative heat loss fractions for the present flames were estimated, using present measurements of laminar smoke point flame lengths, from the correlation of Markstein [26]. This yielded radiative heat loss fractions of 40% for toluene and benzene, and 30% for n-heptane and isopropanol. Fortunately, due to the low values of f for present measurements, values of ρ are relatively independent of heat loss fraction so that these

approximations are not very critical (see Ref. 7 for comparison of results considering and ignoring radiative heat losses).

As anticipated from the results illustrated in Fig. 4, soot generation factors were relatively independent of position for a given flame. Thus, average soot generation factors were computed for each flame and associated with its residence time. Plots of the resulting soot generation factors, as a function of residence time normalized by the smoke point residence time, are illustrated in Fig. 5.

Variations of soot generation factors with residence time in Fig. 5 are all comparable to behavior observed in the long residence time regime for the gas-fueled turbulent diffusion flames [7], i.e., soot generation factors are relatively independent of residence time. This is reasonable, because present flames had residence times that were generally an order of magnitude longer than the smoke point residence time, which was the criterion for the long residence time regime found earlier [7]. The results exhibit relative soot emissions quite concisely, with the greatest soot emitters being toluene and benzene, which are about the same, followed in decreasing order by *n*-heptane and isopropanol. The soot generation factors for toluene and benzene are roughly 0.15, which is somewhat below the value for acetylene, 0.20, measured earlier [7]. The present value of η_s for the liquid alkane *n*-heptane is roughly 0.01, which is essentially the same as the value measured earlier for the gaseous alkane, propane, in the long residence time regime [7], as corrected in Ref. 8. The comparison between the present η_s and those found from the soot yields summarized by Tewarson [2] is considered later.

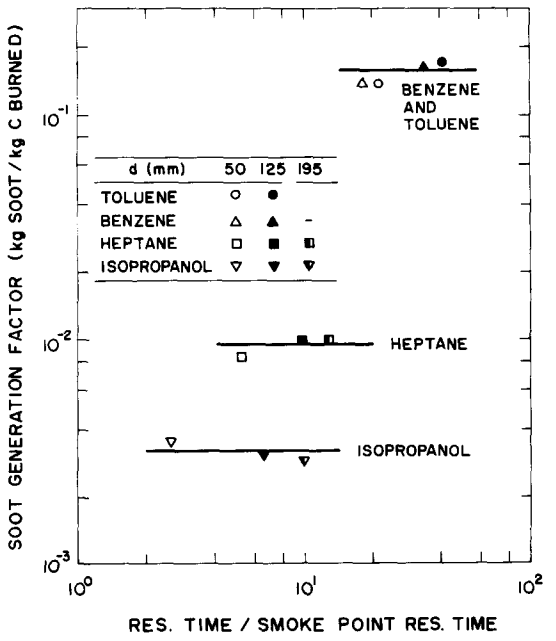

Fig. 5. Soot generation factor as a function of residence time for turbulent toluene, benzene, *n*-heptane, and isopropanol diffusion flames burning in air.

Carbon Monoxide Properties

The gas sampling probe measurements for CO properties were carried out at the same positions as the soot measurements. Proceeding under the assumptions used to find the soot volume fraction state relationships, state relationships also can be constructed for CO concentrations [8]. The resulting measurements and best fit correlations of CO mole fractions as a function of mixture fractions are illustrated in Fig. 6 for toluene, benzene and *n*-heptane, and in Fig. 7 for the alcohols. As before, measurements are only identified by the fuel and the burner diameter to avoid cluttering the figures. Due to the low mixture fraction range of the measurements, the CO state relationship correlations are nearly straight lines, similar to the state relationships for f_s illustrated in Fig. 4.

The carbon monoxide mole fractions plotted in Figs. 6 and 7 exhibit about the same degree of scatter as flame conditions change for a given value of f as f_s in Fig. 4. Additionally, the main trends of the results for X_{CO} and f_s are the same. First of all, results at various positions in the overfire region of any given flame satisfy a linear correlation within experimental uncertainties. Next, results for different burner sizes satisfy nearly the same state relationship, typical of the long-residence time regime of the present flames. Finally, concentrations of CO at particular values of f progressively decrease with decreasing tendency to soot in the order: toluene and benzene (about the same), *n*-heptane, and isopropanol (also about the same), with nonsooting ethanol and methanol having the lowest concentrations of CO.

The effect of flame residence time and the relative propensity to soot on the emission of CO can be examined most concisely by computing

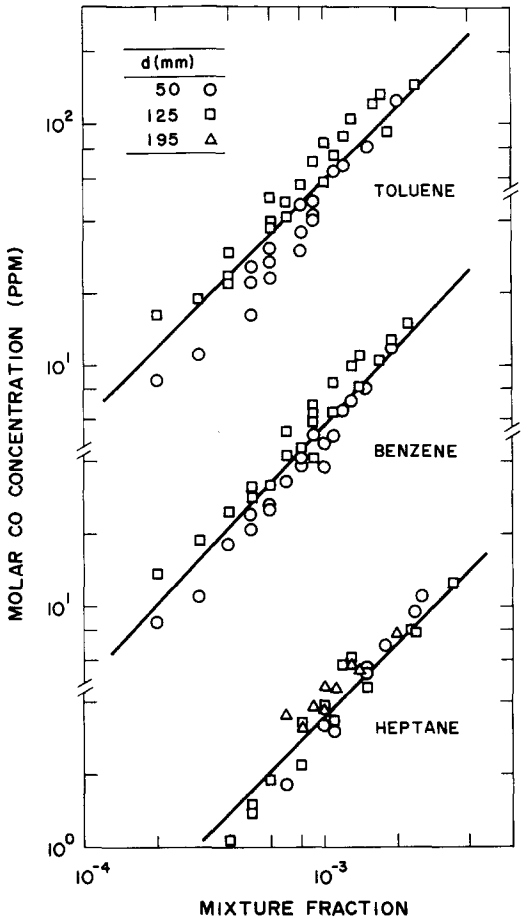

Fig. 6. Carbon monoxide state relationships for the overfire region of turbulent toluene, benzene and *n*-heptane diffusion flames burning in air.

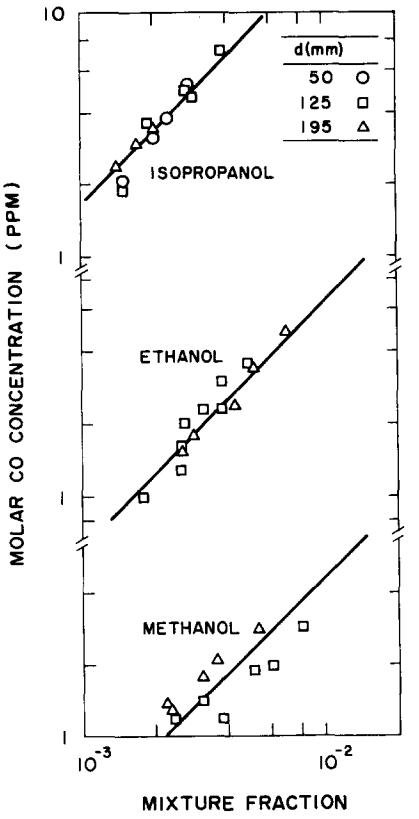

Fig. 7. Carbon monoxide state relationships for the overfire region of turbulent alcohol diffusion flames burning in air.

CO generation factors, η_{CO}. Similar to η_s, η_{CO} should be constant for passive mixing and constant quenching conditions for any flame. Under the same assumptions used to find η_s, η_{CO} can be found from the measured CO and CO_2 concentrations, as follows [8]:

$$\eta_{CO} = M_{CO} X_{CO} / (M_C X_{CO_2}). \quad (9)$$

As noted earlier, η_{CO} values were relatively independent of position in a flame. Thus, an average value of η_{CO} was found for each flame and associated with its residence time. The resulting values of η_{CO} for the sooting fuels are plotted as a function of residence time normalized by the smoke point residence time in Fig. 8 (nonsooting methanol and ethanol will be taken up later). As before, symbols only are identified by fuel type and burner diameter.

Similar to η_s illustrated in Fig. 4, the η_{CO} illustrated in Fig. 8 exhibit relatively little variation with residence time, typical of behavior in the long residence time regime. The similarity between the order of η_s and η_{CO} with fuel type, and their behavior with respect to variations of residence time, is striking and suggests a close relationship between the processes responsible for soot and CO emissions from the present sooting flames, similar to earlier observations for gas-fueled flames [7, 8].

Associating CO and soot emission, however, must be tempered by the observation that methanol and ethanol still emit CO even though they do not emit soot. As suggested by the correlation of measurements of CO concentrations for these flames illustrated Fig. 7, the η_{CO} for these flames were essentially independent of residence time over the present test range, which is typical of behavior in the long residence time regime, e.g., $\eta_{CO} = 0.0012$, with a standard deviation of 0.0004 for both methanol and ethanol. This value

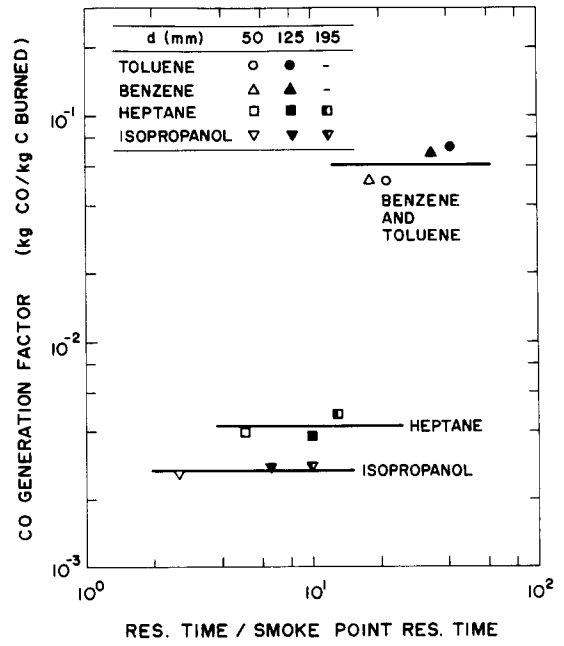

Fig. 8. Carbon monoxide generation factors as a function of residence time for turbulent toluene, benzene, *n*-heptane, and isopropanol diffusion flames burning in air.

is comparable to earlier observations for methane, which is also nonsooting, e.g., $\eta_{CO} = 0.0018$, with a standard deviation of 0.0003 [8]. Thus, CO generation factors for nonsooting fuels are significantly lower than for sooting fuels. This suggests that small emissions of CO that are not associated with soot may still contribute to CO emissions from sooting flames.

Correlation of CO and Soot Emissions

The correlation between CO and soot generation factors is illustrated in Fig. 9. Results shown in Fig. 9 include the present findings for liquid-fueled flames, the earlier findings for gas-fueled flames [7, 8], and results from the extensive tabulation of Tewarson [2]. All the values of η_s involve laser extinction measurements at 632.8 nm, assuming the small particle (Rayleigh scattering) limit, which were reduced to soot volume fractions using the refractive indices of Dalzell and Sarofim [15] and then converted to η_s using the soot density of Newman and Steciak [25]. Measurements from this laboratory are identified by burner size; as noted earlier, flame properties are not identified for the results of Tewarson [2], but these measurements presumably involved large flames in the long residence time regime. Finally, η_{CO} for the nonsooting methane, methanol, and ethanol flames are shown at the left of the plot, to suggest a baseline when η_s is zero.

Except for methane and the alcohols, results illustrated in Fig. 9 exhibit a strong correlation between η_{CO} and η_s. The correlation of measurements from the present laboratory can be quantified reasonably well by the linear fit

$$\eta_{CO} = 0.37\eta_s \tag{10}$$

over the range $0.008 < \eta_s < 0.2$, with standard deviation of the fit over this range of 0.09. A similar fit was found during study of the gas fuel flames over the same range of η_s [8], $\eta_{CO} = 0.34\eta_s$, with a standard deviation of 0.09. In view of the standard deviations of the two expressions, however, their differences are not statistically significant. For $\eta_s > 0.008$, Eq. 10 implies that the mass of fuel carbon leaving the flames as CO and soot divides so that roughly 14% is associated with CO.

Findings for the nonsooting fuels and for the relatively lightly sooting isopropanol indicate that there also is a mechanism for emission of CO from turbulent diffusion flames that is not associated with soot. This mechanism is responsible for all the CO emissions for nonsooting fuels, where averaging measurements from this laboratory for methane, methanol, and ethanol yields.

$$\eta_{CO} = 0.0014, \text{ nonsooting flames}, \tag{11}$$

with a standard deviation of 0.0003. Thus, for these fuels, Eq. 11 implies that roughly 0.06% of the mass of fuel carbon goes into the formation of CO by a nonsooting mechanism.

If the approximation is made that the nonsooting and sooting contributions of CO are simply additive, combining Eqs. 10 and 11 yields

$$\eta_{CO} = 0.0014 + 0.37\eta_s, \tag{12}$$

with standard deviations at the limits of large and small η_s being the same as before. The correlation of Eq. 12 is also illustrated in Fig. 9. It is seen that this relationship provides a reasonable fit of the measurements for weakly sooting isopropanol, e.g., the values of η_{CO} from the measurements and the correlation of Eq. 12 are 0.0027 and 0.0026, respectively. The results tabulated by

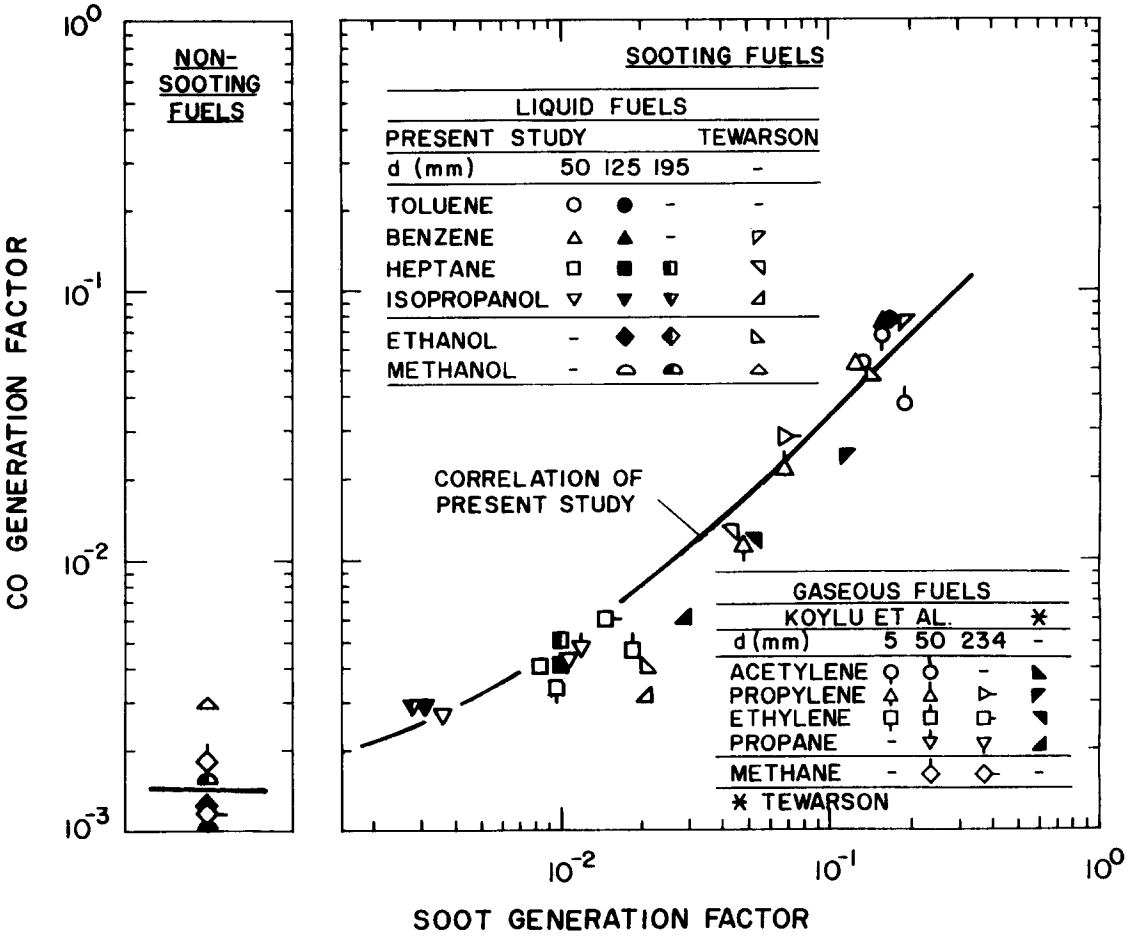

Fig. 9. Carbon monoxide generation factors as a function of soot generation factors for various liquid- and gas-fueled turbulent diffusion flames burning in air. Other data from Tewarson [2] and Köylü et al. [8].

Tewarson [2] and illustrated in Fig. 4 are seen to be in reasonable agreement with Eq. 12 well.

Findings concerning CO and soot emissions of the liquid fuels in the long residence time regime are summarized in Table 3. Entries include η_{CO}, η_s, and their ratio, $\eta_{CO/s} = \eta_{CO}/\eta_s$ (for sooting fuels), which represents the mass of CO emitted per unit mass of soot emitted from the flame. Table 3 also includes values of these parameters from Tewarson [2]. Like Fig. 9, all η_s values were based on extinction measurements using a soot density of 1100 kg/m^3, and involve flames in the long residence regime.

In general, the agreement between present results and those of Tewarson [2] for liquid fuels in Table 3 is much poorer than was observed for the gaseous fuels [8]. The largest discrepancies are for the alcohols, where Tewarson [2] generally indicates much larger emissions of CO and soot than the present study (particularly for methanol and ethanol where the present flames did not emit any soot at all). The reasons for these differences is not known. However, due to the importance of CO and soot emissions from buoyant turbulent flames, additional measurements to evaluate the properties of the liquid fuels given in Table 3, as well as for a broader range of fuels, is clearly merited.

In spite of some quantitative differences, present and earlier findings [8] suggest the presence of sooting and nonsooting mechanisms for the formation of CO. The sooting mechanism appears to involve processes within the soot layer as it passes from fuel-rich to fuel-lean conditions. Certainly, the presence of CO in this layer as long as soot is present, even though CO and soot forma-

TABLE 3

CO and Soot Generation Factors for Liquid Fuels[a]

Fuel	Toluene	Benzene	*n*-Heptane	Isopropanol	Ethanol	Methanol
η_{CO}						
Present	0.063	0.061	0.0042	0.0027	0.0012	0.0012
Tewarson [2]	—	0.070	0.012	0.003	0.004	0.0030
η_s						
Present	0.16	0.15	0.0095	0.0032	0.00	0.00
Tewarson [2]	—	0.19	0.044	0.023	0.023	< 0.003
$\eta_{CO/s}$						
Present	0.394	0.407	0.422	0.844	—	—
Tewarson [2]	—	0.368	0.273	0.130	0.174	> 1.00

[a] Present results for the long residence-time regime. All η_s estimated from optical measurements using a soot density of 1100 kg/m^3.

tion mechanisms in the layer are certainly not the same, is reasonable based on past work: in the fuel-rich region, the soot layer (or soot spike) just on the fuel-rich side of stoichiometric involves maximum concentrations of both CO and soot in the flame [7, 13]; soot generally oxidizes to CO as a first step and OH plays a strong role in oxidizing both CO and soot [1, 6] so that the continued presence of soot implies the continued presence of CO as well; and radiative heat losses from soot implies lower temperatures as the soot layer passes from fuel-rich to fuel-lean conditions than at other points along the flame sheet, which should contribute to reduced rates of oxidation of CO and help to quench reactions before CO oxidation is complete. Recent measurements in the soot layer of laminar flames tend to support this general picture, suggesting that competition between CO and soot for the oxidizer species OH can be responsible for high CO emissions from sooting flames, with radiative quenching (to reduce OH) possibly important in fuel-lean regions [6].

In In addition to emission of CO associated with the soot layer, however, conventional emission of CO from regions of the flame sheet not crossed by the soot layer is also expected. This involves quenching of CO oxidation reactions as temperatures drop when moving away from the flame sheet toward fuel-lean conditions, followed by passive mixing in the overfire region. This mechanism would explain the low level CO emissions from the nonsooting fuels but probably contributes to some extent to CO emissions from sooting fuels as well. Nevertheless, the sooting mechanism of CO emissions is generally dominant for sooting flames. This helps explain the limited success of past attempts to predict CO emissions from turbulent diffusion flames which ignore the presence of soot [27], although these methods still may be helpful for treating the nonsooting CO mechanism.

CONCLUSIONS

Soot and carbon monoxide emissions were studied for overventilated buoyant turbulent diffusion flames involving liquid fuels (toluene, benzene, *n*-heptane, isopropanol, ethanol, and methanol) burning in still air. The main conclusions of the study are as follows:

1. Similar to earlier findings for sooting gaseous fuels (acetylene, propylene, ethylene and propane), soot and CO generation factors were uniform throughout the overfire region for a given fuel and operating condition, implying both passive mixing in the overfire region and constant conditions when soot and CO oxidation reactions quench—independent of position in the flame.
2. Present measurements for sooting flames involved flame residence times generally an order of magnitude larger than the laminar smoke point residence time. Then, similar to the gas-fueled flames [7, 8], soot and CO generation factors were relatively independent of flame residence time in this long residence time regime.
3. Nonsooting methanol and ethanol flames exhibited lower levels of CO emissions than the sooting flames but their CO generation factors

also were uniform over the overfire region and were relatively independent of residence time (for residence times greater than 245 ms).

4. The correlations between CO and soot emissions could be represented as $\eta_{CO} = 0.0014 + 0.37\eta_s$ from measurements in this laboratory for both gas [7, 8] and liquid fuels. This suggests sooting and nonsooting mechanisms for CO emissions from flames, with the former dominating CO emissions from sooting flames. The sooting mechanism is associated with processes within the soot layer as it passes from fuel-rich to fuel-lean conditions; it is conjectured that the nonsooting mechanism involves quenching of CO oxidation reactions on the fuel-lean side of the flame sheet in regions where the soot layer does not cross the flame sheet.
5. Present measurements of CO and soot generation factors for the liquid fuels were in much poorer agreement with the tabulation of Tewarson [2] than was observed earlier for gaseous fuels [7, 8] (particularly for methanol and ethanol, which did not emit soot during present measurements but are listed as soot emitters in [2]). The reason for this behavior is not known. Additional measurements of soot and CO emissions from buoyant turbulent diffusion flames are needed to help resolve these discrepancies and to study the relationships between CO and soot emissions for a broader range of materials representative of the environment of unwanted fires.

This research was supported by the Center for Fire Research of the National Institute of Standards and Technology, Grant No. 60NANB8D033, with H. R. Baum serving as Scientific Officer.

REFERENCES

1. Friedman, R., *Fire Safety Science: Proceedings of the First International Symposium*, Hemisphere, Washington, 1986, p. 349.
2. Tewarson, A., in *SFPE Handbook of Fire Protection Engineering*, National Fire Protection Association, Quincy, MA, 1988, pp. 1-179.
3. Tewarson, A., and Newman, J. S., *Fire Safety Science: Proceedings of the First International Symposium*, Hemisphere, Washington, 1986, p. 451.
4. Fischer, S. J., and Grosshandler, W. L., *Twenty-Second Symposium (International) on Combustion*, The Combustion Institute, Pittsburgh, 1988, p. 1241.
5. McCaffrey, B. J., and Harkleroad, M., *Twenty-Second Symposium (International) on Combustion*, The Combustion Institute, Pittsburgh, 1988, p. 1251.
6. Puri, R., and Santoro, R. J., *Fire Safety Science: Proceedings of the Third International Symposium*, Hemisphere, Washington, in press.
7. Sivathanu, Y. R., and Faeth, G. M., *Combust. Flame* 81:133-149 (1990).
8. Köylü, Ü. Ö., Sivathanu, Y. R., and Faeth, G. M., *Fire Safety Science: Proceedings of the Third International Symposium*, Hemisphere, Washington, in press.
9. Bilger, R. W., *Combust. Flame* 30:277-284 (1977).
10. Sivathanu, Y. R., and Faeth, G. M., *Combust. Flame* 82:211-230 (1990).
11. Schug, K. P., Manheimer-Timnat, T., Yaccarino, P., and Glassman, I., *Combust. Sci. Technol.* 22:235-250 (1980).
12. Flower, W. L., and Bowman, C. T., *Twenty-First Symposium (International) on Combustion*, The Combustion Institute, Pittsburgh, 1986, p. 1115.
13. Gore, J. P., and Faeth, G. M., *J. Heat Transf.*, 110:173-181 (1988).
14. Santoro, R. J., Dobbins, R. A., and Semerjian, H. G., *Prog. Astronaut. Aeronaut.* 92:343-382 (1984).
15. Dalzell, W. H., and Sarofim, H. F., *J. Heat Transf.* 91:100-104 (1969).
16. Gore, J. P., Ph.D. thesis, The Pennsylvania State University, University Park, PA, 1986.
17. Zukoski, E. E., Cetegen, B. M., and Kubota, T., *Twentieth Symposium (International) on Combustion*, The Combustion Institute, Pittsburgh, 1984, p. 361.
18. Olson, D. B., Pickens, J. C., and Gill, R. J., *Combust. Flame* 62:43-60 (1985).
19. Clarke, A. E., Hunter, T. G., and Garner, F. H., *Inst. Petrol.* 32:627 (1946).
20. Steward, F. R., *Combust. Sci. Technol.* 2:203-212 (1970).
21. Thomas, P. H., *Ninth Symposium (International) on Combustion*, The Combustion Institute, Pittsburgh, 1962, p. 844.
22. You, H.-Z., and Faeth, G. M., *Fire Materials* 3:140-147 (1979).
23. Drysdale, D., *An Introduction to Fire Dynamics*, Wiley, New York, 1985, p. 126.
24. Glassman, I., *Twenty-Second Symposium (International) on Combustion*, The Combustion Institute, Pittsburgh, 1988, p. 295.
25. Newman, J. S., and Steciak, J., *Combust. Flame* 67:55-64 (1987).
26. Markstein, G. H., *Twentieth Symposium (International) on Combustion*, The Combustion Institute, Pittsburgh, 1984, p. 1055.
27. Bilger, R. W., and Stårner, S. H., *Combust. Flame* 51:155-176 (1983).

Received 29 March 1991; revised 26 June 1991